Int. J. Adv. Res. Sci. Technol. Volume 15, Issue 9, 2026, pp. 2606-2611.

IJARST

International Journal of Advanced Research in Science and Technology

https://doi.org/10.62226/ijarst20262817

ISSN 2319 – 1783 (Print)

ISSN 2320 – 1126 (Online)

Adaptive Formation Reconfiguration and Artificial Potential Field Avoidance for Multi UAVs in Constrained Spaces

Shuo Yang[1], Xinyi Li*[2]

1 China North Vehicle Research Institute, Beijing, 100072, Beijing, China.

2 School of Automation, Nanjing University of Science and Technology, No. 200 Xiaolingwei, Nanjing, 210094, Jiangsu, China

Email:tiexue66666@163.com

ARTICLEINFO

Article history:

Received	10 Sep 2026
Accepted	18 Sep 2026
Available online	21 Sep 2026

Keywords:

Multi UAVs, Formation reconfiguration, Virtual leader, Artificial potential field, Obstacle avoidance, Collision avoidance

Indexed in:

doi Crossref

INDEX COPERNICUS INTERNATIONAL

Google scholar

and in major libraries

ABSTRACT

Multi-UAV formations operating in constrained environments must balance formation maintenance and local obstacle avoidance. Fixed formation geometry may become unsuitable when obstacles restrict lateral clearance, whereas abrupt formation switching can generate tracking transients. This paper proposes a virtual-leader-based adaptive formation control method that integrates restricted-space recognition, smooth formation reconfiguration, artificial potential field avoidance, inter-UAV repulsion, and speed constraints. The controller selects a V-shaped or single-file reference according to the surrounding obstacle configuration. A smoothing mechanism is introduced to ensure continuous transition between formation geometries, while the control input is continuously updated from formation-tracking, obstacle-repulsion, and collision-avoidance terms. Simulations on a multi-UAV simulation platform verify the proposed method in constrained and obstacle-rich environments. The formation can switch to a compact single-file configuration in restricted regions and recover the V formation after passing the obstacles. The results show that the controller maintains coordinated formation motion, avoids recorded obstacle contact, preserves inter-UAV separation, and keeps UAV speeds within the prescribed range.

Introduction

Multi-UAV formations are widely used for tasks requiring spatial coverage and coordinated motion, with formation control often organized through virtual structures or leader-following frameworks[1][2][3]. In open space, a V-shape provides good lateral separation, but it becomes restrictive in narrow passages or when obstacles flank the route[4][5]. The conflict is twofold: each UAV must avoid obstacles while staying close to its formation reference; rigid formation holding can cause incompatible commands, while abrupt geometry changes induce large tracking errors.

Artificial potential field (APF) methods offer direct local avoidance commands and are attractive for real-time control[6], but they do not provide global planning and may suffer from local minima[7]. Many existing formation studies assume fixed geometries or separate obstacle-replanning layers[8], with less attention paid to smooth reconfiguration driven by environmental narrowness.

This paper contributes a continuous controller with three linked functions: detecting restricted passages from obstacle positions, applying smoothed transitions between V-shape and single-file offsets, and generating commands from tracking, regularized repulsion, inter-UAV repulsion, and speed bounds. Simulations verify the method in two obstacle scenarios, reporting formation mode, tracking errors, and safety distances.

Related Work:

1. Formation control and virtual leaders

Formation control may be organized through leader following, virtual structures, behavior-based interaction, or consensus based coordination. Consensus formulations describe how local information exchange can produce common motion in a networked group. Leader following formulations introduce a moving reference and specify offsets for the remaining agents[2]. For fixed wing or multirotor UAV teams, this representation is useful because the leader trajectory and the formation geometry can be treated separately. The present controller follows this convention: the virtual leader specifies forward motion, while the offsets specify the desired local geometry.

2. Potential fields and local avoidance

Potential field navigation represents the target as an attractive influence and obstacles as repulsive influences[4]. The approach is simple to implement, but the force grows rapidly when a distance variable approaches zero. It can also become trapped in unfavorable obstacle geometry. Navigation functions and global planning methods were developed to address broader classes of obstacle environments. This paper does not substitute a local potential field for these methods. Instead, it uses a regularized distance to prevent numerical singularity.

3. Gap addressed in this study

Many formation studies examine a prescribed geometry or a single avoidance mechanism. The practical difficulty in a narrow passage is that the formation itself must become part of the avoidance response. The gap addressed here is therefore not a claim of a new global planner. It is the integration of a simple restricted space decision rule, a smooth V shape to single file transition, and local APF control in one simulation model with reported distance and speed measures.

Control Method

1. Formation model and control objective

The formation is represented by one virtual leader and N follower UAVs. For follower i, p_i and v_i denote its position and velocity, and u_i is the acceleration command generated by the cooperative controller. The leader position and velocity are p_l and v_l. At the upper-control level, each follower is represented by the second-order kinematic model

$$\frac{dp_i}{dt} = v_i, \qquad \frac{dv_i}{dt} = u_i$$

(0)

The desired position of follower i is defined relative to the virtual leader as

$$p_i^d = p_l + o_i$$

(1)

where o_i is the active formation offset. The controller selects either the V-formation offset set O_V or the single-file offset set O_L.

The individual position tracking error and formation-Centre error are respectively defined

$$e_i = p_i - p_i^d, \qquad p_c = \frac{1}{N}\sum_{i=1}^{N} p_i, \qquad e_c = \left\| p_c - p_c^d \right\|$$

(2)

Here, p_c is the actual formation Centre and p_c^d is the Centre implied by the leader and the current reference geometry. The control objective is to make e_i decrease after a manoeuvre while retaining local obstacle avoidance and inter-UAV separation. The paper addresses the upper-level command-generation problem only; it does not claim an aircraft attitude controller or a global route planner. Figure 1 summarizes the control structure.

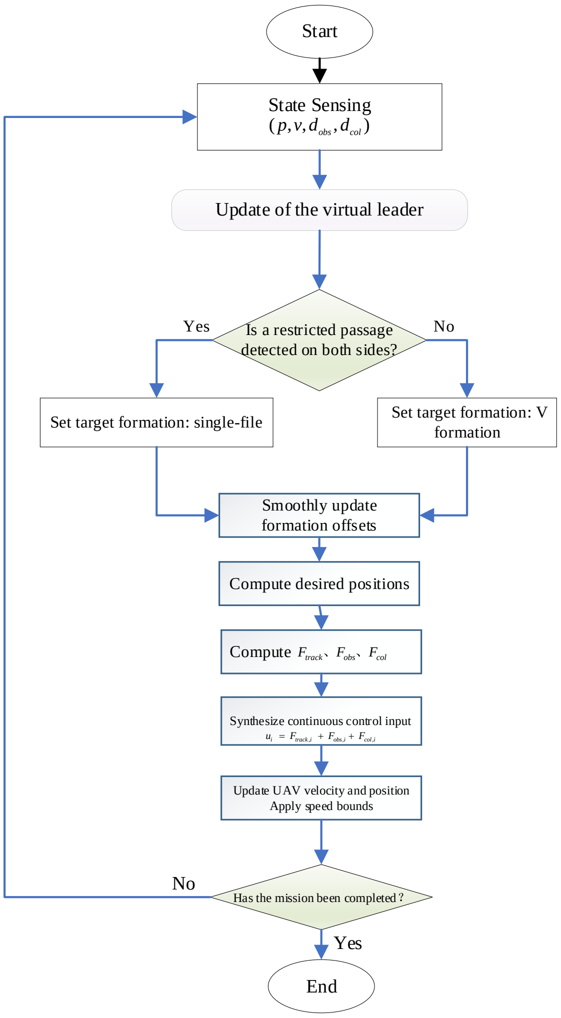

Figure 1. Control architecture linking restricted space detection, formation reference update, and local force generation.

2. Virtual leader motion and adaptive speed

The virtual leader supplies a common forward reference while maintaining the prescribed flight-height layer. Let d_f be the unit forward direction. The leader speed is regulated by the formation-Centre error rather than kept fixed. Its scalar speed and velocity are defined as

$$v_l^s = v_{ref} e^{-\lambda_s \frac{\max(0, e_c - E_{th})}{L}}$$

(3)

$$v_l = v_l^s d_f, \qquad \frac{dp_l}{dt} = v_l$$

(3)In (4), v_{ref} is the nominal cruise speed, E_{th} is the admissible formation-Centre error before deceleration is introduced, L is a normalization constant, and λ_s controls sensitivity. When e_c is small, the leader travels close to the nominal speed. As e_c increases, the reference moves more slowly and gives the followers time to recover their relative positions. This is a coordination mechanism only: obstacle detouring is produced by the local potential-field terms described below.

3. Restricted-space recognition and smooth formation reconfiguration

Obstacle geometry is interpreted in the moving frame defined by the virtual leader. For obstacle j with Centre c_j, the leader-relative vector and its forward and lateral components are

$$r_l j = c_j - p_l, s_j = r_l j^T d_f, q_j = r_l j^T d_r \quad (4)$$

Where d_r is the lateral unit direction. An obstacle is considered relevant only when it lies ahead of the leader and within the prescribed detection range. The restricted-space flag is activated when valid obstacles are identified on both sides of the forward route. Let $b_L(k)$ and $b_R(k)$ be binary indicators of valid obstacle detection on the left and right sides, respectively.

$$\chi(k) = b_L(k) b_R(k) \quad (5)$$

If a valid left obstacle and a valid right obstacle are both detected $\chi(k) = 1$, otherwise $\chi(k) = 0$.

The target offset set then follows the switching rule

$$\begin{aligned} O_{tar(k)} &= O_L, if\ \chi(k) = 1; \\ O_{tar(k)} &= O_V, if\ \chi(k) = 0. \end{aligned} \quad (6)$$

An isolated obstacle can therefore activate local repulsion without forcing the whole formation into single file. To prevent a discontinuity in the desired positions when the target geometry changes, the active offsets evolve as

$$O(k) = (1-\lambda_f) O(k-1) + \lambda_f O_{tar(k)}, 0 < \lambda_f < 1$$
(7)

The smoothing factor λ_f determines how rapidly the active geometry approaches the selected target. Equation (9) ensures that the desired positions change continuously; the resulting transition is then executed by the tracking controller rather than by an instantaneous position change.

4. Artificial potential field control law

The desired velocity used by the tracking term is the current leader velocity. The formation-tracking term combines a position-restoring component and a velocity-damping component:

$$v_i^d = v_l, F_t rack, i = K_p (p_i^d - p_i) + K_v (v_i^d - v_i) \quad (8)$$

For a spherical obstacle, d_ij is the distance from UAV i to the obstacle surface and n_ij is the outward unit vector from the obstacle Centre to the UAV:

$$d_{ij} = \|p_i - c_j\| - r_j, n_{ij} = \frac{p_i - c_j}{\|p_i - c_j\|} \quad (9)$$

The obstacle term is active only when d_ij is smaller than the obstacle influence distance d_{obs}. To avoid numerical singularity of the inverse-distance expression, the controller replaces d_{ij} by the regularized value

$$d_{\text{reg},ij} = \max(d_{ij}, d_{\min}) \quad (10)$$

The corresponding obstacle repulsion is

$$F_{\text{obs},i} = \begin{cases} \sum_{j=1}^{N_{\text{obs}}} K_{\text{obs}} \left(\frac{1}{d_{\text{reg},ij}} - \frac{1}{d_{\text{obs}}} \right) \frac{1}{d_{\text{reg},ij}^2} n_{ij}, & d_{ij} < d_{\text{obs}}, \\ 0, & d_{ij} \geq d_{\text{obs}} \end{cases} \quad (13)$$

The regularization in (12) protects the numerical calculation only. It does not redefine the physical contact boundary, which remains $d_{ij} = 0$. The influence distance d_{obs} is therefore not described as a collision boundary.

5. Inter-UAV separation, continuous update, and scope

To prevent collisions among formation members, an inter-UAV repulsive potential field is introduced. For UAV i and UAV m, the relative distance and the unit vector directed from UAV m to UAV i are defined as

$$d_{im} = \|p_i - p_m\|, n_{im} = \frac{p_i - p_m}{d_{im}} \quad (11)$$

When the distance between two UAVs becomes smaller than the prescribed collision-avoidance activation distance d_{col}, a repulsive acceleration is generated. The inter-UAV collision-avoidance term is expressed as

$$F_{\text{col},i} = \begin{cases} \sum_{\substack{m=1 \\ m \neq i}}^{N} K_{\text{col}} \left(\frac{1}{d_{im}} - \frac{1}{d_{\text{col}}} \right) \frac{1}{d_{im}^2} n_{im}, & d_{im} < d_{\text{col}}, \\ 0, & d_{im} \geq d_{\text{col}} \end{cases} \quad (12)$$

Here, K_{col} is the inter-UAV repulsion gain. The repulsive term increases rapidly as d_{im} decreases, directing the two UAVs away from each other. In this study, d_{col} is the activation distance of the collision-avoidance term.

The final control input is obtained by superposing the formation-tracking term, the obstacle-avoidance term, and the inter-UAV collision-avoidance term:

$$u_i(k) = F_{\text{track},i}(k) + F_{\text{obs},i}(k) + F_{\text{col},i}(k) \quad (13)$$

The control command is updated at every sampling instant. The velocity and position of UAV i are updated as

$$\begin{aligned} v_i(k+1) &= v_i(k) + u_i(k)\Delta t, \\ p_i(k+1) &= p_i(k) + v_i(k+1)\Delta t \end{aligned} \quad (13)$$

To maintain the commanded speed within the allowable flight range, the updated velocity is constrained by

$$\|v_i(k+1)\| \in [v_{\min}, v_{\max}] \quad (14)$$

Thus, the proposed controller recalculates the control input continuously at each sampling instant.

Simulation Design

Initial condition and obstacle environments

The simulation considers five UAVs over a 32 s interval. All vehicles begin in the V formation and follow a virtual leader moving along a constant-height route. The experiment includes two obstacle environments. The first is a narrow passage formed by a pair of large obstacles on both sides of the route. It tests whether the controller changes from the V formation to the single-file formation and then restores the V formation. The second contains separated smaller obstacles. It tests the local avoidance response and the return to the nominal formation after the obstacle region.

Table 1 summarizes the main simulation parameters, including the number of UAVs and simulation duration, speed bounds, tracking gains, obstacle and inter-UAV repulsion settings, and the formation smoothing factor. These parameters are kept fixed in both obstacle scenarios to evaluate the proposed controller.

Table 1. Simulation parameters.

Group	Parameter	Value
Formation	Number of UAVs; duration	5; 32 s
Speed	Lower; reference; upper speed	10; 25; 40 m/s
Tracking	Position and velocity gains	5.0; 6.0
Obstacle field	Repulsion gain; influence distance	2000; 25 m
Inter-UAV field	Repulsion gain; activation distance	350; 8 m
Formation update	Smoothing factor	0.1

Results and Analysis

1. Three-dimensional flight trajectory

Figure 2 shows the three-dimensional trajectories of the five UAVs. The trajectories progress through the two obstacle environments without an abrupt loss of formation continuity. Around the restricted region, the lateral distribution of the vehicle's contracts; after passing the obstacles, the trajectories become approximately parallel again.

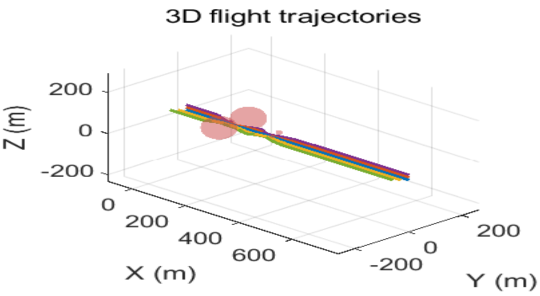

Figure 2. Three-dimensional flight trajectories of the five UAVs.

2. Formation snapshots

Figure 3 presents representative snapshots before, within, and after the two obstacle environments. In the narrow-passage snapshots, the formation compresses into the single-file geometry. In the separated-obstacle snapshots, the vehicles make local adjustments around the obstacles and then recover the V configuration. These panels provide the most direct geometric view of the formation-reconfiguration process and should be read together with the trajectory and mode records that follow.

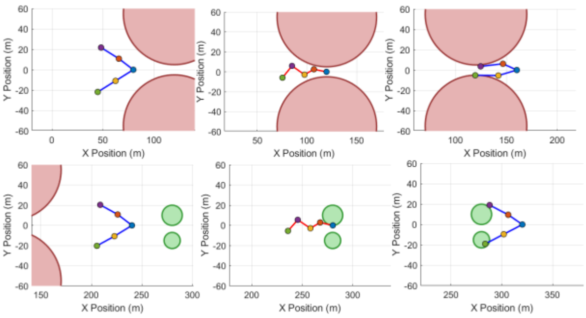

Figure 3. Representative formation snapshots before, during, and after the two obstacle environments.

3. Horizontal-plane trajectory

Figure 4 presents the horizontal-plane trajectories together with the obstacle outlines. The path deviations occur locally near the obstacle regions rather than persisting throughout the route. In the narrow passage, the formation follows the available corridor. In the separated-obstacle environment, each UAV makes a small local adjustment and then returns toward the nominal forward route. The plot therefore provides a direct planar view of the APF avoidance response.

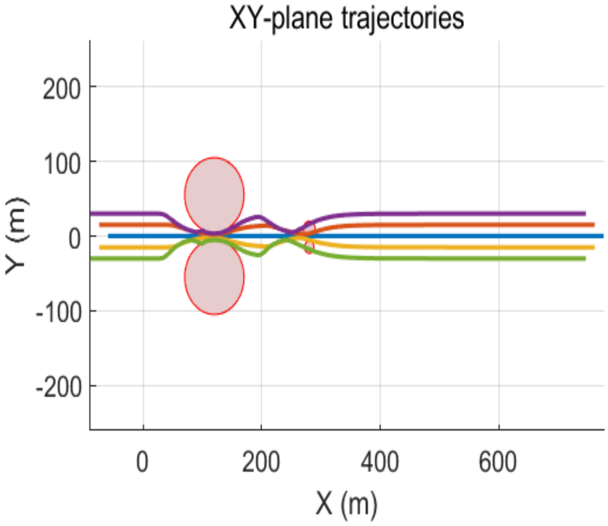

Figure 4. Horizontal-plane trajectories and obstacle outlines.

4. Formation-mode transition

Figure 5 gives the formation-mode history. The controller enters the single-file mode twice, approximately during 3-6 s and 10-12 s, when the restricted-space condition is detected. It subsequently returns to, and remains in, the V formation. This record verifies that the compact formation is used locally rather than being maintained after the restricted regions are passed.

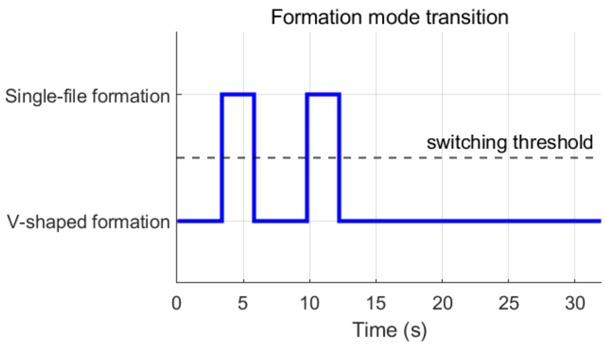

Figure 5. Formation-mode transition during the simulation.

5. Position tracking error

Figure 6 shows the position tracking error of each UAV. The errors increase during initial convergence and during the two formation transitions because the desired geometry changes while the vehicles are moving. After each transition, the errors decrease. By about 16 s, all five curves are close to zero. This recovery is consistent with the purpose of the smoothed offset update: it avoids a permanent displacement mismatch after the formation reference changes.

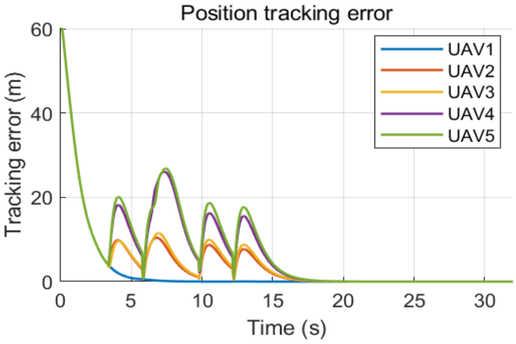

Figure 6. Position tracking errors of the five UAVs.

6. Velocity tracking error

Figure 7 shows the velocity tracking error. Its peaks occur in the same periods as the position-error transients, reflecting the acceleration needed to follow the changing reference and avoid obstacles. The curves decay after the local manoeuvres and approach zero in the later part of the run.

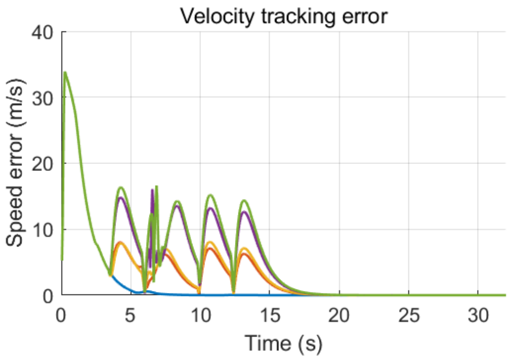

Figure 7. Velocity tracking errors of the five UAVs.

7. Minimum inter-UAV distance

Figure 8 illustrates the minimum pairwise distance among the five UAVs throughout the simulation. The inter-UAV distance decreases during the formation reconfiguration and obstacle-avoidance manoeuvres, reaching a minimum value of 10.114 m. This value remains above the prescribed collision-avoidance activation distance of 8 m, indicating that the simulated formation does not enter the inter-UAV repulsion activation region. After the local manoeuvres are completed, the minimum distance gradually recovers to approximately 21 m, which is close to the initial formation separation. The result indicates that the formation reconfiguration and local obstacle avoidance processes do not cause excessive compression of the UAV spacing in the simulated scenarios.

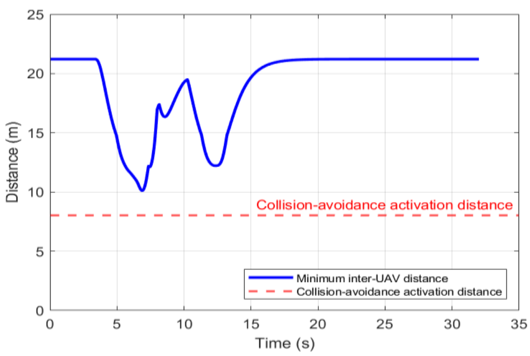

Figure 8. Minimum inter-UAV distance during the simulation. The red dashed line denotes the collision-avoidance activation distance.

Table 2 summarizes the key performance measures, including control effort, speed range, safety distances, and formation mode proportions. The results show that the speed remains within the prescribed bounds, the obstacle surface distance stays positive, and the inter-UAV distance remains above the repulsion activation threshold. The formation stays in the V shape for most of the simulation and switches to single file only locally. Overall, the controller satisfies the speed and separation constraints while achieving local formation reconfiguration.

Table 2. Recorded performance measures.

Measure	Recorded value	Interpretation within this simulation
Mean control acceleration	5.478 m/s²	Transient control effort
Minimum UAV speed	16.642 m/s	Above 10 m/s lower bound
Maximum UAV speed	40.000 m/s	Equal to 40 m/s upper bound
Initial minimum inter UAV distance	21.213 m	Initial geometric separation
Minimum obstacle surface distance	1.360 m	Above zero collision boundary
Minimum inter UAV distance	10.114 m	Above 8 m activation distance
V shape / single file time	85.0% / 15.0%	Compact mode used locally

Conclusion

This paper presented a virtual leader based multi UAV formation controller for two local obstacle environments. The controller selects a V shape or single file target from the relative obstacle geometry, smooths the transition between offset sets, and combines tracking, regularized obstacle repulsion, inter UAV repulsion, and speed constraints in each update.

In simulations of five UAVs, the formation completed two single file transitions, returned to the V shape, avoided obstacle surface contact, and maintained a minimum inter UAV distance of 10.114 m. The speed record remained within 16.642 to 40.000 m/s. These observations support the controller for the two specified local environments.

References

[1] Hu Jiawei, Jia Zequn, Sun Yantao, et al. Analysis of Multi-UAV Cooperative Mission Planning under Multi-Constraint Conditions and a Review of Solution Methods [J]. Computer Science, 2023, 50(07): 176-193.

[2] Askari A, Mortazavi M, Talebi H A. UAV formation control via the virtual structure approach[J]. Journal of Aerospace Engineering, 2015, 28(1): 04014047.

[3] Lu Jun, Yang Jie, Hao Yongping, et al. Leader-Follower-Based Collision-Avoidance Flight Control for UAV Formations [J]. Journal of Shenyang University of Technology, 2024, 43(04): 38-43+50.

[4] Cao Xiaoyi, Luo Xuqiong, Li Jing, et al. A Path Planning Method for Multi-UAV Formations Based on an Improved Artificial Potential Field Approach [J]. Computer Applications, 2025, 45(S1): 183-187.

[5] Q. Yang, J. Yan, X. Yang and X. Luo, Multi-AUV Formation Control Based on Combination of Artificial Potential Field and Virtual Structure[C]//2023 42nd Chinese Control Conference (CCC). IEEE, 2023:5247-5252.

[6] Z. Zhou, X. Xing, Y. Li and R. Wang, Multi-UAV Path Planning Based on Potential Field Dense Reward in Unknown Environments with Static and Dynamic Obstacles[C]//2023 China Automation Congress (CAC). IEEE, 2023:1289-1294.

[7] Tang C, Ji L, Yang S, et al. Prescribed-time containment control of multi-agent systems subject to collision avoidance and connectivity maintenance[J]. ISA Transactions, 2024, 148: 156-168.

[8] J. Ge, C. Fan, C. Yan and L. Wang, Multi-UAVs close formation control based on wild geese behavior mechanism[C]//2019 Chinese Automation Congress (CAC). IEEE, 2019:967-972.